Research Article Vol. 7, No. 8 / August 2020 / Optica 1015

Exceptional points in polaritonic cavities and subthreshold Fabry–Perot lasers

Jacob B. Khurgin

Johns Hopkins University, Department of ECE, Baltimore, Maryland 21218, USA (jakek@jhu.edu)

Received 11 May 2020; revised 5 July 2020; accepted 12 July 2020 (Doc. ID 397378); published 14 August 2020

We show that concept of parity-time (PT) symmetry can be expanded to include mixed photon-exciton modes by demonstrating that eigenmodes of active (pumped) strongly coupled cavity polaritons with population inversion exhibit characteristics that are remarkably akin to those of coupled photonic structures with parity-time symmetry. The exceptional point occurs when the Rabi splitting of polariton branches inherent in passive polaritonic systems decreases with increase in pumping, leading to population inversion, and eventually two polaritonic modes merge into a single mode, thus manifesting the frequency pulling effect inherent to all lasers. But, remarkably, this exceptional point occurs below the lasing threshold. Furthermore, unlike most manifestations of PT symmetry in optics, which are observed in the interaction between two analogous photonic modes in waveguides or cavities, in this work the exceptional point is found in interaction between two very dissimilar modes—one photonic and one material excitation (exciton). Aside from fundamentally noteworthy expansion of the concept of PT symmetry to new systems, there is a prospect of using the exceptional point in polaritons for practical applications, such as sensing.

https://doi.org/10.1364/OPTICA.397378

1. INTRODUCTION

Every student of quantum mechanics is familiar with the postulate that the Hamiltonian of the physical system must be Hermitian in order to make certain that the eigenvalues are real. This notion, however, has been challenged in last few decades, when it has been shown that a system described by a non-Hermitian Hamiltonian can also have real eigenvalues as long as that Hamiltonian satisfies the combined conditions of parity-time (PT) symmetry [1]. Thus, the field of non-Hermitian quantum mechanics was born, and from that point it has been the focus of attention of many theorists [2–4]. In particular the interest has been aroused by the existence of the exceptional points (EPs) at the boundary between the regions where PT symmetry is preserved and broken [5] and where the eigenfunctions of the Hamiltonian become degenerate. While the theoretical progress of PT studies has been spectacular, experimental observation of non-Hermitian but PT symmetric properties in Nature has remained elusive. But the phenomena related to PT symmetry have been manifested in other branches of physics, most prominently in photonics. This development was in a certain way inevitable, as the wave equations governing quantum mechanics and optics are closely related, and hence a photonic system can be an excellent simulator of a quantum mechanical one [6] as has been exploited by finding optical counterparts to such condensed matter concepts as band theory [7], Anderson localization [8], and topological phenomena [9], among others. An entire cottage industry of replicating quantum mechanical phenomena in optics [10] has since sprung up and blossomed. Hence, it was only a matter of time until first the theoretical works [11–14] and then reports of observation of PT-like phenomena in photonics, including EPs, started appearing [15,16] in the literature. From there on, PT symmetry has been demonstrated in large variety of photonic structures—coupled waveguides, coupled resonators, lasers [17], Bragg grating [18], etc. as described in a number of excellent reviews [19–21]. In particular, the EPs [22] where the phase transitions occur have been observed, and, most encouragingly, it was shown that in the vicinity of EPs the sensitivity of various sensors [23–25] can be enhanced, which may potentially lead to practical applications, although, given the inherent instability of any system near phase transitions [26], there are still a lot of obstacles on the path to widespread application of PT-symmetric photonics.

A couple of general observations can be made about all the photonic structures in which PT symmetry and EPs have been observed or theoretically shown to exist. First, in all cases the coupled modes comprising the PT system are of the same photonic nature—typically, the modes in coupled waveguides, coupled microresonators, or forward and backward modes in ring resonators or gratings. Second, the structures are specifically designed to satisfy PT symmetry conditions, which is usually done be carefully adjusting the loss and gain in them. It is somewhat disappointing to note that the vast majority of PT symmetry experiments use structures that have almost no reason for their existence other than demonstrating PT symmetry with perhaps some added functionality. That includes all the works on PT symmetry in lasers [17,27–29], where specially designed multimode or coupled lasers with alternating gain and loss regions needed to be employed.

Needless to say, it would be intriguing to identify a photonic structure that is ubiquitous and is extensively used in many photonics systems today, and in which the PT symmetry properties and in particular EPs can be observed "as is" and considered as an added functionality. Furthermore, from the fundamental physics point of view, it would be instructive to consider a PT-symmetric structure in which the coupled modes that comprise it are of very different physical origins [30]. In this work we demonstrate that such system exists and that PT symmetry and EPs can be observed in a well-known system comprised by the ensemble of two-level atoms (or exciton) placed in a microcavity and pumped (optically or electrically) but below the lasing threshold. So one can think of this system schematically shown in Fig. 1 as either an active polariton in a Fabry–Perot microcavity [31] or as a subthreshold vertical cavity surface emitting laser (VCSEL) [32]. We show that two kinds of conditions for EPs can be identified in this system—one below and one above the transparency. Of course these structures have been extensively studied, and the phenomena occurring near EPs, namely, polaritonic Rabi splitting in the regime of strong coupling on one hand [33,34] and frequency pulling in the lasers [35] on the other, are obviously familiar to most students of photonics. Still, in our view, it is worthwhile to look at familiar structures from a different angle and to discover that the most fundamental phenomenon of coupling between matter and light can produce EPs as has been shown in [30], and that by changing pumping, the system can be tuned to be either at an EP or encircle it. Besides being a scientific curiosity, this study may even lead to practical applications in sensing, but in that respect we shall try to refrain from being carried away and try to remain concentrated on science.

2. COUPLED LIGHT–MATTER EQUATIONS

As mentioned above, we study a Fabry–Perot microcavity [36], shown in Figs. 1(a) and 1(b) with an optically active resonant medium in it. For the purpose of generality, the active medium is described as a two-level ensemble of atoms with transition energy $\hbar\omega_{21}$ and the dephasing rate γ_{21} whose density is $N(\boldsymbol{r})$. In practice, the active medium is typically a semiconductor or an organic medium in which the transition is an excitonic one, but one can always describe it using a two-level model. For example, if the active medium is a multiple quantum well (MQW) structure [37,38], shown in Fig. 1(c), the density of equivalent two-level atoms can be found as $N(\boldsymbol{r}) = 2|\Phi_{\rm ex}(0)|^2 \sum_n^{N_{\rm QW}} \delta(z - z_n)$, where $\Phi_{\rm ex}(0)$ is the value of excitonic wavefunction at the origin and z_n is the plane of one of the $N_{\rm QW}$ quantum wells. The active medium can then be described by a set of density matrix equations for the population of lower and upper levels ρ_{11}, ρ_{22} and coherences ρ_{21}, ρ_{12}:

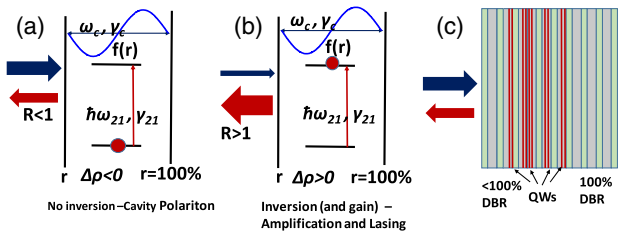

Fig. 1. Polaritonic system comprised by a Fabry–Perot cavity with a resonant medium pumped (a) below and (b) above transparency. (c) Specific implementation of this system with semiconductor multiple quantum wells placed in cavity comprised by two distributed Bragg reflectors (DBRs).

$$\begin{aligned}
\frac{d\Delta\rho(\boldsymbol{r})}{dt} &= -\left(\Delta\rho - \Delta\rho_p\right)/T_1 + j\frac{\boldsymbol{\mu}_{21}\cdot\boldsymbol{E}(\boldsymbol{r})}{\hbar}(\rho_{21} - \rho_{12}),\\
\frac{d\rho_{21}}{dt} &= -\gamma_{21}\rho_{21}(\boldsymbol{r}) - j\omega_{21}\rho_{21}(\boldsymbol{r}) + j\frac{\boldsymbol{\mu}_{21}\cdot\boldsymbol{E}(\boldsymbol{r})}{\hbar}\Delta\rho,\\
\rho_{21}(\boldsymbol{r}) &= \rho_{12}^*(\boldsymbol{r}),
\end{aligned} \tag{1}$$

where $\Delta\rho = \rho_{11} - \rho_{22}$, $\Delta\rho_p$ is the equilibrium value of $\Delta\rho$ maintained by pumping, T_1 is the population relaxation rate, $\boldsymbol{\mu}_{21}$ is the matrix element of the dipole transition, and $\boldsymbol{E}(\boldsymbol{r})$ is the optical field inside the cavity;

$$E(\boldsymbol{r}, t) = A(t)\boldsymbol{f}(\boldsymbol{r})e^{-j\omega t} + \text{c.c.}, \tag{2}$$

where $f(bfr)$ is the normalized shape of the mode that satisfies $\int f^2(\boldsymbol{r})\mathrm{d}V = 1$ and the Helmholtz equation

$$\nabla^2\boldsymbol{f} + n^2\frac{\omega_c^2}{c^2}\boldsymbol{f} = 0, \tag{3}$$

and ω_c is the cavity resonance frequency. Note that we can introduce the effective volume of the cavity as $V_{\rm eff} = 1/f_{\rm max}^2$, and then $|A|^2(t) = |E_{\rm max}|^2/V_{\rm eff}$. We assume that the optical field is weak so we can neglect the saturation phenomena, the population density is uniform, and there is constant $\Delta\rho(t, \boldsymbol{r}) \equiv \Delta\rho_p$. Pumping can be accomplished optically via a four-level pumping scheme or electrically by carrier injection. In the ensemble of two-level atoms (or, equivalently, in Frenkel exciton) the change in $\Delta\rho$ means that some of the atoms are in the excited state. For a Wannier exciton, the situation is more complex, and change $\Delta\rho$ means a combination of state filling and screening of Coulomb interaction by the carriers [39]. Introducing the rotating wave approximation $\rho_{21} = e^{-j\omega t}\sigma_{21}$ and substituting it into Eq. (1), one obtains the expression for the coherence:

$$\begin{aligned}
\frac{d\sigma_{21}(\boldsymbol{r})}{dt} &= -\gamma_{21}\sigma_{21}(\boldsymbol{r}) - j(\omega_{21} - \omega)\sigma_{21}(\boldsymbol{r})\\
&\quad + j\frac{A\boldsymbol{\mu}_{21}}{\hbar}\cdot\boldsymbol{f}(\boldsymbol{r})\Delta\rho.
\end{aligned} \tag{4}$$

Next we can introduce the collective dipole excited in the medium by the optical field as

$$p = \int \boldsymbol{\mu}_{21}\cdot\boldsymbol{f}(\boldsymbol{r})N(\boldsymbol{r})\sigma_{21}(\boldsymbol{r})\mathrm{d}V \tag{5}$$

and integrate equation over the volume to obtain

$$\frac{dp}{dt} = -\gamma_{21}p - j(\omega_{21} - \omega)p + j\frac{\mu_{21}^2 A\Delta\rho}{\hbar}N_{\rm eff}. \tag{6}$$

Here μ_{21} is a projection of the atomic dipole onto the direction of the optical field, and $N_{\rm eff} = \int N(\boldsymbol{r})f^2(\boldsymbol{r})\mathrm{d}V$ is the effective density of atoms. For the case of excitons in a MQW structure, where the quantum wells are inserted in the Bragg reflector, $N_{\rm eff} = 2|\Phi_{\rm ex}(0)|^2 N_{\rm QW}/L_{\rm eff}$, where $L_{\rm eff}$ is the effective width of the mode. The optical field is governed by the wave equation

$$\nabla^2\boldsymbol{E}(t, \boldsymbol{r}) - \frac{n^2}{c^2}\frac{\partial^2}{\partial t^2}\boldsymbol{E}(t, \boldsymbol{r}) = \frac{1}{c^2}\frac{\partial^2}{\partial t^2}\frac{\boldsymbol{P}(t, \boldsymbol{r})}{\varepsilon_0}, \tag{7}$$

where material polarization $\boldsymbol{P}(\boldsymbol{r}) = \boldsymbol{\mu}_{21}\sigma_{21}(\boldsymbol{r})N(\boldsymbol{r})$. Substituting and using the eigenmode condition, one obtains

$$-\omega_c^2 \boldsymbol{f}(\boldsymbol{r})A + \omega^2 \boldsymbol{f}(\boldsymbol{r})E + 2j\omega \boldsymbol{f}(\boldsymbol{r})\frac{\partial A}{\partial t} = -\frac{\omega^2 \boldsymbol{\mu}_{21}\sigma_{21}(\boldsymbol{r})N(\boldsymbol{r})}{\varepsilon_0 \varepsilon}. \tag{8}$$

Multiplication of by $\boldsymbol{f}(\boldsymbol{r})$ and integration over the volume then yields

$$2j\omega\frac{\partial A}{\partial t} = \left(\omega_c^2 - \omega^2\right) A - \frac{\omega^2}{\varepsilon_0 \varepsilon} p, \tag{9}$$

close to resonance $\omega_c^2 - \omega^2 \approx 2\omega(\omega_c - \omega)$. Multiplying by $-j$ and adding some dissipation, we obtain in combination with

$$\begin{aligned} \frac{\partial A}{\partial t} &= -j(\omega_c - \omega)A - \gamma_c A + j\kappa_1 p, \\ \frac{dp}{dt} &= -\gamma_{21} p - j(\omega_{21} - \omega)p + j\kappa_2 A, \end{aligned} \tag{10}$$

where the coupling coefficients are $\kappa_1 = \omega/2\varepsilon_0\varepsilon$ and $\kappa_2 = \mu_{21}^2 \Delta\rho N_{\text{eff}}/\hbar$. Now we introduce $\kappa^2 = \kappa_1\kappa_2 = \kappa_0^2\Delta\rho$, where the coupling coefficient for the ground state (unpumped) polariton is

$$\kappa_0^2 = \frac{\mu_{21}^2 \omega}{2\varepsilon_0 \varepsilon_r \hbar} N_{\text{eff}} = f_{21}\frac{e^2}{4m_0\varepsilon_0\varepsilon_r} N_{\text{eff}} = f_{21}\omega_p^2/4, \tag{11}$$

f_{21} being an oscillator strength of the transition and ω_p plasma frequency, which indicates that the whole phenomenon can be treated classically as well as quantum mechanically. Note that when the population inversion condition $\Delta\rho < 0$ is reached, κ^2 becomes negative, meaning that coupling coefficient κ becomes imaginary and the Hamiltonian becomes non-Hermitian even in the absence of damping.

Finally, we introduce dimensionless variables

$$\begin{aligned} a &= \sqrt{\frac{2\varepsilon_0\varepsilon_r}{\hbar\omega}} A = \sqrt{\frac{2\varepsilon_0\varepsilon_r V_{\text{eff}}}{\hbar\omega}} E_{\max}, \\ b &= \frac{p}{\mu_{21} N_{\text{eff}}^{1/2} \Delta\rho^{1/2}} = \frac{\int N(\boldsymbol{r})\sigma_{21}(\boldsymbol{r}) f(\boldsymbol{r}) \mathrm{d}V}{\sqrt{\Delta\rho \int N(\boldsymbol{r}) f^2(\boldsymbol{r}) \mathrm{d}V}}, \end{aligned} \tag{12}$$

and obtain coupled-mode equations

$$\begin{aligned} j\frac{\partial a}{\partial t} &= (\omega_c - \omega - j\gamma_c)a - \kappa b, \\ j\frac{db}{dt} &= (\omega_{21} - \omega - j\gamma_{21})b - \kappa a, \end{aligned} \tag{13}$$

where a is the photon amplitude, or, essentially a photon creation operator, and b is the amplitude of a collective dipole (or exciton), i.e., an exciton creation operator. The latter can be seen by assuming uniform field distribution in the active region and then obtaining $b \approx N_{\text{tot}}^{1/2}\sigma_{21}/\Delta\rho$, where N_{tot} is the total number of atoms inside the cavity (for excitons in MQW $N_{\text{tot}} \approx N_{\text{eff}} = 2|\Phi_{\text{ex}}(0)|^2 N_{\text{QW}} S$, where S is the resonator area). This fact indicates coherent addition of all the individual dipoles. Normalization to $\Delta\rho$ becomes important when $\Delta\rho \sim 0$. Of course, $|a|^2$ and $|b|^2$ are the Hopfield coefficients representing relative weights of photon and matter (exciton) in the polariton. Note that since the total number of atoms inside the cavity N_{tot} is large and $|b| \le 1$, the magnitude of the off-diagonal matrix element $|\rho_{21}| \approx \Delta\rho N_{\text{tot}}^{-1/2}|b| \ll 1$, and therefore, according to the Rabi oscillations of polarization, do not affect the population inversion, which remains $\Delta\rho \approx \Delta\rho_p$.

3. FROM RABI SPLITTING TO LASING THRESHOLD

The characteristic equation of Eq. (13) of is

$$\begin{vmatrix} \omega_c - \omega - j\gamma_c & -\kappa \\ -\kappa & \omega_{21} - \omega - j\gamma_{21} \end{vmatrix} = 0, \tag{14}$$

and the solutions for the complex frequencies $\tilde{\omega}_{1,2} = \omega_{1,2} - j\gamma_{1,2}$ are

$$\tilde{\omega}_{1,2} = \bar{\omega} - j\bar{\gamma} \pm \sqrt{(\Delta\omega - j\Delta\gamma)^2 + \kappa_0^2\Delta\rho}, \tag{15}$$

where $\bar{\omega} = (\omega_c + \omega_{21})/2$, $\bar{\gamma} = (\gamma_c + \gamma_{21})/2$, $\Delta\omega = (\omega_c - \omega_{21})/2$, and $\Delta\gamma = (\gamma_c - \gamma_{21})/2$. The EP occurs when the expression under the square root is equal to zero. And exactly when EP occurs depends on the sign of $\Delta\rho$. For positive $\Delta\rho$, the EP can only appear if the two-level atom (or exciton) is resonant with the cavity, so that

$$\tilde{\omega}_{1,2} = \omega_c - j\bar{\gamma} \pm \sqrt{\kappa_0^2\Delta\rho - (\Delta\gamma)^2}, \tag{16}$$

and the pair of EPs occurs when $\Delta\gamma = \pm|\kappa| = \pm\kappa_0\Delta\rho^{1/2}$. These two EPs designated as EP1 are shown in Fig. 2 in normalized coordinates $\delta\omega = \Delta\omega/|\kappa|$ and $\delta\gamma = \Delta\gamma/|\kappa|$.

For the negative $\Delta\rho$, i.e., under population inversion condition, the EP occurs when the decay rates of the exciton and photon are equal $\gamma_{21} = \gamma_c$ so that

$$\tilde{\omega}_{1,2} = \bar{\omega} - j\bar{\gamma} \pm \sqrt{(\Delta\omega)^2 - \kappa_0^2|\Delta\rho|}, \tag{17}$$

and the pair of EPs, designated as EP2 and also shown in Fig. 2, appear when $\Delta\omega = \pm|\kappa| = \pm\kappa_0|\Delta\rho|^{1/2}$. Note that when population inversion is present at EP2, the Hamiltonian of the system has a rather interesting form with real diagonal elements and imaginary but not conjugated off-diagonal ones:

$$H = \begin{pmatrix} \Delta\omega & j\kappa \\ j\kappa & -\Delta\omega \end{pmatrix}. \tag{18}$$

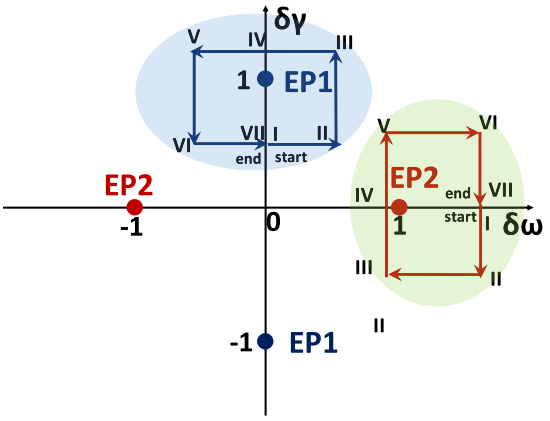

Fig. 2. Exceptional points in the cavity–matter system without (EP1) and with (EP2) population inversion. Frequency detuning $\delta\omega$ and the difference of damping constants between the cavity and exciton $\delta\gamma$ are normalized to the absolute value of coupling strength. Also shown are the encirclement pathways discussed in Section 5.

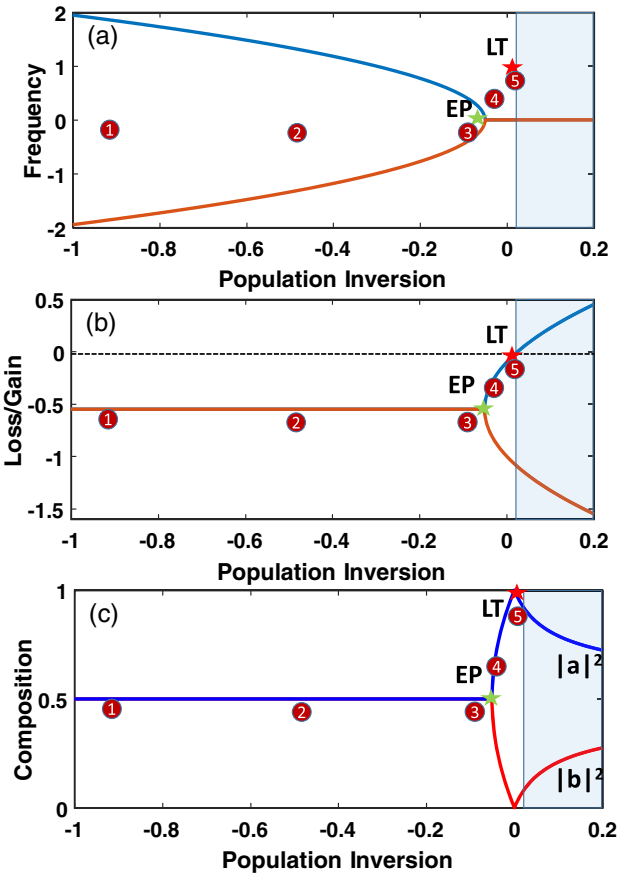

Fig. 3. Polaritonic modes of the cavity–matter system with $\omega_c = \omega_{21} = 0$, $\gamma_{21} = 0.7$, $\gamma_c = 0.4$, and $\kappa_0 = 2.0$: (a) resonant frequencies $\omega_{1,2}$, (b) damping rates $-\gamma_{1,2}$, (c) Hopfield coefficients $|a|^2$ (photon) and $|b|^2$ (material excitation) versus population inversion $-\Delta\rho$. EP, exceptional point (of the first kind); LT, laser threshold. The tinted region is inaccessible due to gain saturation and clamping at the threshold value. Numbers 1–5 correspond to the reflectivity spectra in Fig. 5.

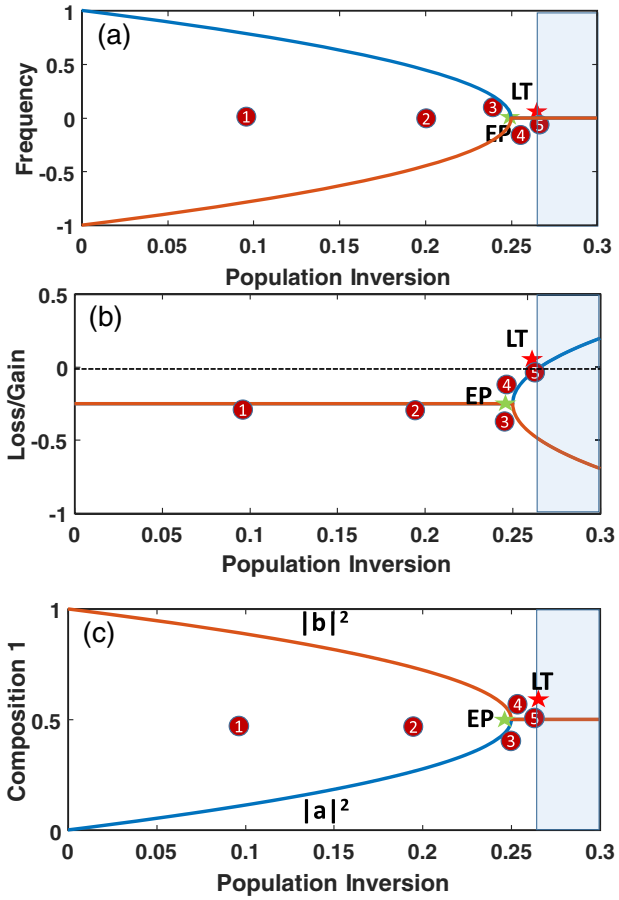

Fig. 4. Polaritonic modes of the cavity–matter system with $\omega_{21} = -\omega_c = 1$, $\gamma_{21} = \gamma_c = 1.0$, $\gamma_c = 0.1$, and $\kappa_0 = 2.0$ pumped into the population inversion region: (a) resonant frequencies $\omega_{1,2}$, (b) damping rates $-\gamma_{1,2}$, (c) Hopfield coefficients $|a|^2$ (photon) and $|b|^2$ (material excitation) versus population inversion $-\Delta\rho$. EP, exceptional point (of the second kind); LT, laser threshold. The tinted region is inaccessible due to gain saturation and clamping at the threshold value. Numbers 1–5 correspond to the reflectivity spectra in Fig. 6.

The characteristics of the cavity–exciton system without and with population inversion are illustrated in Figs. 3 and 4, respectively. In Fig. 3 the first case is considered, i.e., $\omega_c = \omega_{21} = 0$ (relative to the cavity resonance), $\gamma_{21} = 1.0$, $\gamma_c = 0.1$, and $\kappa_0 = 2.0$, all in relative units. The real (i.e., resonant frequency) and imaginary (i.e., net loss or gain) part of frequency is plotted versus population inversion, i.e., $-\Delta\rho$. As one can see, in the absence of pumping $-\Delta\rho = -1$, two distinct solutions with equal Hopfield coefficients (50:50 mixture of photon and matter excitation) and equal damping rates $\bar{\gamma}$ are present, but at EP $\Delta\rho_{\mathrm{EP}} = |\Delta\gamma|/\kappa_0$ these two solutions become fully degenerate, and following that point, both solutions have the same resonant frequency but different damping rates and different Hopfield coefficients. Once $\Delta\rho$ becomes negative, i.e., population inversion is reached, the damping rate of one of the solutions (the one that contains mostly photons) decreases, and eventually reaches zero at the laser threshold (LT). At this point lasing commences, and further increase of population inversion becomes impossible—hence, the region beyond LT is tinted in Fig. 3.

In Fig. 4 we consider a different situation, when the damping rates of photons in the cavity and in the matter are equal ($\gamma_c = \gamma_{21} = 0$), but the frequencies are detuned ($\omega_{21} = -\omega_c = 1$), while coupling is kept at $\kappa_0 = 2.0$. For this case we consider only the region with population inversion $-\Delta\rho > 0$. As one can see at zero population inversion there are two uncoupled modes, but as population inversion increases, the two modes start mixing, and at the EP become fully degenerate. Then, as population inversion increases, even further one of the coupled modes (symmetric) becomes less and less lossy until the LT is reached at which point population inversion becomes clamped. The fact that above laser threshold the frequency of the lasing mode is pulled towards gain maximum is well known [40], but that it happens below threshold and that EP is reached below the threshold are less familiar and quite important from both fundamental and practical points of view.

4. HOW TO OBSERVE THE EP?

The next question is how the evolution of the polariton system can be observed. Obviously one should monitor the transmission and reflection of the cavity while population inversion changes. The measurement is easier if the cavity has one of the mirrors close to 100% as shown in Fig. 1(c), i.e., it is a Gires–Tornois interferometer (GTI) [41], since absorption and reflection are complementary, and therefore only either one of these

characteristics needs to be monitored. The reflectivity of the GTI is

$$R = \left| \frac{e^{j\Phi} - r}{1 - re^{j\Phi}} \right|^2, \tag{19}$$

where r is the amplitude reflection coefficient of the front mirror, and the round-trip phase shift in the vicinity of order cavity resonance is

$$\Phi(\omega) = 2m\pi + \tau_{rt}\left[\omega_c \frac{\delta n(\omega)}{n} + (\omega - \omega_c)\right], \tag{20}$$

where τ_{rt} is the cavity round-trip time, $\omega_c \tau_{rt} \equiv 2m\pi n$ is the refractive index in the absence of resonant medium, and $\delta n(\omega)$ is the change of index caused by the resonant medium, which can be found as

$$\delta n = \frac{1}{2n} \frac{N_{\text{eff}} \mu_{21}^2 \Delta\rho}{\varepsilon_0 \hbar[(\omega_{21} - \omega) - j\gamma_{21}]}$$

$$= n \frac{\kappa_0^2 \Delta\rho}{\omega[(\omega_{21} - \omega) - j\gamma_{21}]}, \tag{21}$$

and where Eq. (11) has been used. Using and relating the cavity damping rate to the front mirror reflectivity as $r = \exp(-\gamma_c \tau_{rt})$, the reflectivity can be found as

$$R = \left| \frac{e^{j\tilde{\Phi}}/r - r}{1 - e^{j\tilde{\Phi}}} \right|^2, \tag{22}$$

where the complex phase is

$$\tilde{\Phi}(\omega) \approx 2m\pi + \tau_{rt}\left[\frac{\kappa_0^2 \Delta\rho}{(\omega_{21} - \omega) - j\gamma_{21}} - (\omega_0 - \omega - j\gamma_c)\right]. \tag{23}$$

It is clear that the resonances occur when $\tilde{\Phi}(\omega) = 2m\pi$, and equating the term in the square brackets to zero leads us to precisely the characteristic equation. Also, this equation can be used to find the laser threshold condition by postulating that the solution of the characteristic equation is real, i.e., that the imaginary part of the determinant is zero, i.e., $\gamma_c(\omega_{21} - \omega) = -\gamma_{21}(\omega_c - \omega)$, and

$$\omega = \frac{\gamma_c \omega_{21} + \gamma_{21} \omega_c}{\gamma_c + \gamma_{21}}, \tag{24}$$

which is of course the textbook case of frequency pulling [40]. With that, the threshold condition is

$$-\kappa_0^2 \Delta\rho = \gamma_c \gamma_{21}\left[\frac{(\omega_{21} - \omega_c)^2}{(\gamma_{21} + \gamma_c)^2} + 1\right]. \tag{25}$$

Let us now look at the reflectivity spectra of the first polaritonic system at five different values of population inversion all shown by red circles in Fig. 3. The results are shown in Fig. 5(a).

Indeed, one can observe how two distinct Rabi split modes (1,2) gradually get closer to each other until they merge at EP (3), where $\Delta\rho = (\Delta\gamma)^2/\kappa_0^2$, while reflectivity at the resonance decreases until it reaches 0 at point 4, where $\Delta\rho = \gamma_c\gamma_{21}/\kappa_0^2$, where the perfect absorption (or, more prosaically, impedance matching, is achieved). Once population inversion takes place, the reflectivity exceeds unity meaning that reflected light gets amplified inside the cavity, and near threshold the reflectivity approaches

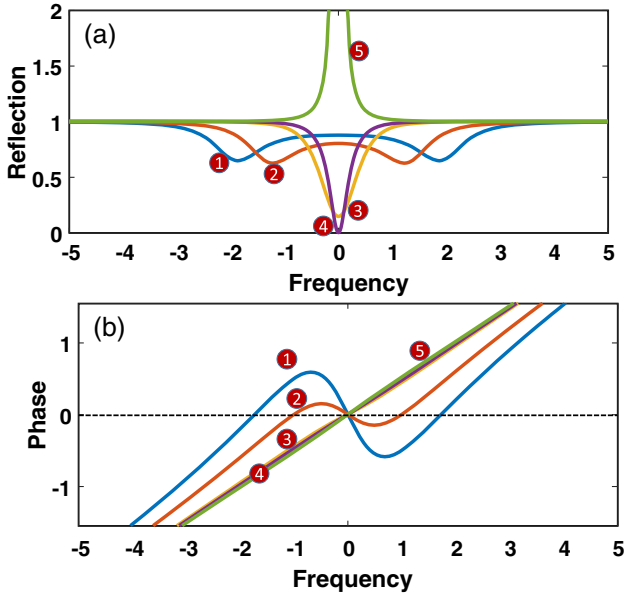

Fig. 5. Spectra of (a) reflectivity R and (b) real part of the round-trip phase shift $\text{Re}\tilde{\Phi}(\omega)$ at five different values of population inversion for the polaritonic system of Fig. 3.

infinity, meaning that amplification turns into self-sustained oscillations. Note that the threshold is reached when $\Delta\rho = -\gamma_c\gamma_{21}/\kappa_0^2$, i.e., at the value equal in magnitude and opposite in sign to the population inversion at perfect absorption. This truism flows naturally out of the reciprocity principle, and it lends a degree of credence to the mundane act of impedance matching being newly looked upon as a novel and somewhat esoteric phenomenon of "antilasing" [42].

In Fig. 5(b) the spectra of the real part of the phase $\tilde{\Phi}(\omega) - 2\pi m$ is plotted. As one can see, for the unpumped, or weakly pumped, cases (1) and (2), the phase curve has an N-shaped region in the vicinity of cavity resonance, so the phase curve intersects the horizontal axis three times, leading to three solutions, of which the middle one can be shown to be unstable and the other two correspond to two polariton branches. But as one approaches EP, the negative slope region slowly disappears, and only one solution remains. Obviously, for the medium with inversion, the N shape turns upside down, and only one solution is possible. In other words, the lasing can only take place at one frequency near the exciton transition and not at one of the two polariton branches. (Note that here we are talking about the conventional "photon" lasing with population inversion, which should not be confused with an entirely different "polaritonic lasing" phenomenon occurring at far lower pump powers [43,44]).

Next we take a look at the reflectivity and phase spectra for the EP of the second kind (Fig. 4), with EP occurring with the positive inversion. The reflectivity spectra are shown in Fig. 6(a), and one can see how at relatively low values of inversion and gain the cavity acts as a regenerative amplifier at two polariton modes, but then these two modes merge near EP. Thus, regenerative amplification is possible at polariton frequencies, but not lasing. The phase spectra of Fig. 6(b) confirm this fact. Note that in case of amplification, even if the real part of phase indicates resonance in the vicinity of ω_{21}, it does not mean that resonance can be exploited for lasing.

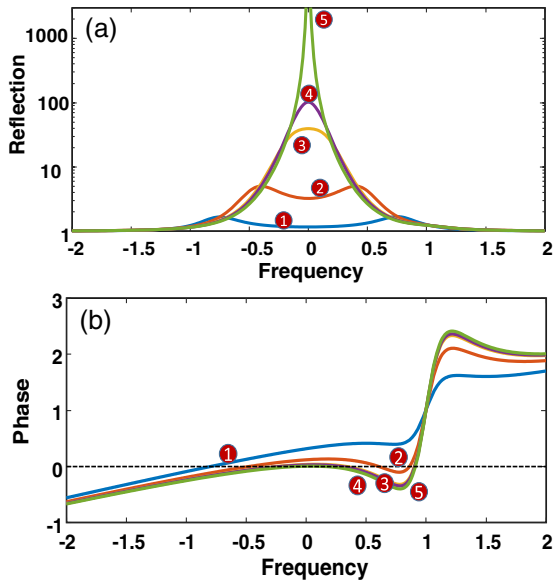

Fig. 6. Spectra of (a) reflectivity R and (b) real part of the round-trip phase shift $\mathrm{Re}\tilde{\Phi}(\omega)$ at five different values of population inversion for the polaritonic system with inversion of Fig. 4.

5. EP ENCIRCLEMENT

The narrative of the EP would not be complete unless we also probed the possibility and observability of the encirclement around EP and associated with it "flipping" of the eigenstates. Adiabatic encirclement of the EPs has been first studied in Refs. [45,46], and it was predicted that each time the adiabatic encirclement took place it will cause a flip of eigenstates. That has been confirmed in a number of "quasi-static" experiments where the eigenstates were monitored while slowly and discretely changing the parameters of the system [47–49]. But later on it was shown, theoretically, that when the encirclement occurs dynamically the fact that the Hamiltonian of the system is non-Hermitian (i.e., in optics it involves loss and gain) prevents one from applying the adiabatic theorem, and the encirclement of the EP results in a different final state that depends only on the direction (helicity) of the encirclement and not on the initial state [50–53]. The dynamic encirclement was first experimentally demonstrated in coupled microwave waveguides in 2016 [54].

We have performed the parametric study of encirclement of the EPs in a cavity–matter arrangement. First we have considered the EP of the fist kind, in a system without inversion around the exceptional point of the first kind EP1 occurring at $\gamma_c = 0.1$, $\gamma_{21} = 1$, $\kappa^2 = .45$, $\Delta\omega = 0$ as shown in Fig. 2, blue contour. The results of the encirclement are shown in Fig. 7. At the start of the encirclement (point I), one can observe two identical Rabi-split modes with their eigenfrequencies [Fig. 7(a)] well separated and decay rates, plotted relative to the mean decay rate $\bar{\gamma}$ [Fig. 7(b)], equal to each other. The Hopfield coefficients [Fig. 7(c)] of both modes are equal to $1/2$, indicating that each mode contains equal contributions from the photon and matter (exciton). The reflectivity spectrum [Fig. 7(d)] shows two distinct reflectivity dips corresponding to two modes. Then, as the detuning $\Delta\omega$ increases, the modes are pulled apart (point II). The higher frequency mode (blue) has photon-like character and lower loss—hence, in the reflectivity spectrum of Fig. 7(d) this mode has a sharper dip. As the difference in decay rates $\Delta\gamma$ starts growing

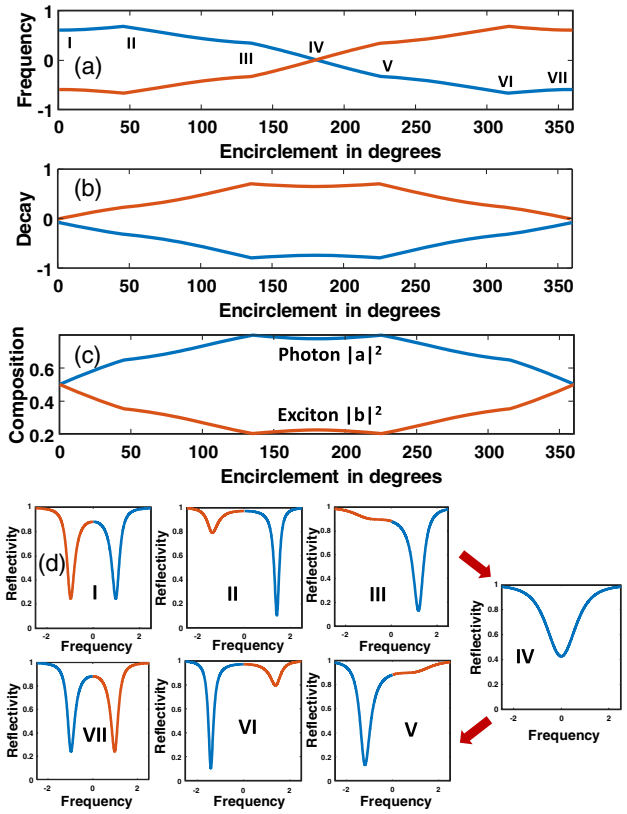

Fig. 7. Encirclement of the EP of the first kind along the pathway shown in Fig. 2: (a) frequencies normalized to $|\kappa|$, (b) damping rates (relative to the mean), (c) Hopfield coefficients, and (d) evolution of the reflectivity spectrum.

(point III), the splitting gets reduced and the asymmetry between two deeps increases, then as detuning $\Delta\omega$ decreases further (point IV), the frequencies of two modes become equal, but one of the modes is about 80% pure photon character, and therefore the observed dip is due to that mode. Once the sign of $\Delta\omega$ changes, that low-loss mode moves to lower frequencies, eventually splits from the other mode (point V), and then grows sharper (point VI) as the loss is further decreased. Finally, upon completion of full circle (point VII), the mode becomes the lower frequency mode in full accord, thus accomplishing a state flip.

Next consider encirclement in system with inversion, around the exceptional point of the second kind EP2 occurring at $\gamma_c = \gamma_{21} = 0.4$, $\kappa^2 = -.15$, $\Delta\omega = 1$ as shown in Fig. 2, red contour. The results of the encirclement are shown in Fig. 8. At the start of the encirclement (point I), one can observe two modes with their eigenfrequencies [Fig. 8(a)] well separated and decay rates, plotted relative to the mean decay rate $\bar{\gamma}$ [Fig. 8(b)], equal to each other, even though the Hopfield coefficients [Fig. 8(c)] of both modes are different. The reflectivity spectrum [Fig. 8(d)] shows two distinct reflectivity (gain) peaks corresponding to two modes. Then, as the decay rate of the higher frequency (photon-like) mode gets smaller (point II), that mode (shown in blue) shows a higher peak in the reflectivity spectrum. The two peaks then get closer (point III) as the detuning $\Delta\omega$ decreases. Then, as the decay rates of the two modes become equal (point IV), the peaks merge (even though the frequencies of the uncoupled cavity and exciton are very different), and the reflectivity grows as the laser approaches the threshold but never gets there. Note that the reflectivity at

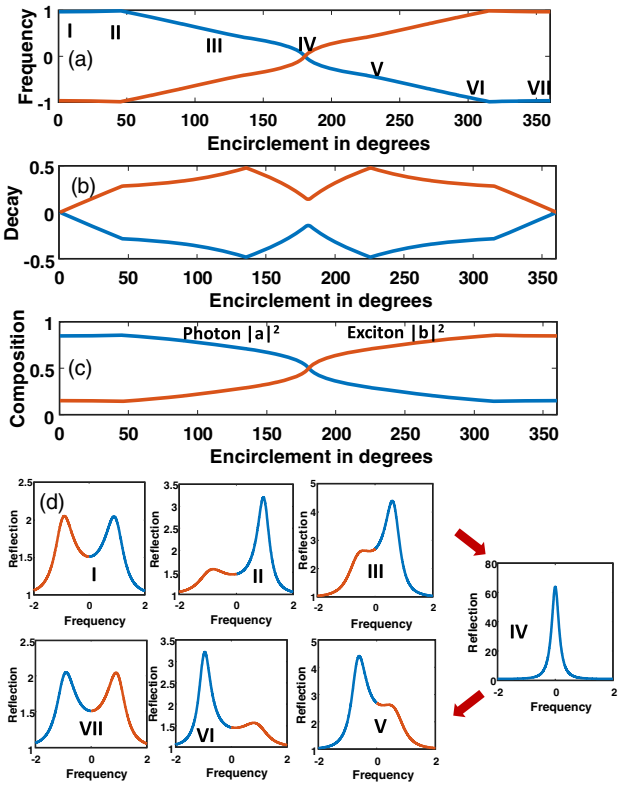

Fig. 8. Encirclement of the EP of the second kind (with gain) along the pathway shown in Fig. 2: (a) frequencies normalized to $|\kappa|$, (b) damping rates (relative to the mean), (c) Hopfield coefficients, and (d) evolution of the reflectivity spectrum.

this point exceeds 50, i.e., the system acts as a regenerative optical amplifier with a large gain. Once the decay rate of the exciton becomes less then the decay rate of photon, it is the exciton-like mode that shows a stronger peak (points V,VI), and eventually that mode is on the low-frequency side of the reflectivity spectrum, which thus completes the state flip (point VII).

While the results of our quasi-static analysis indicate fully symmetric state flip, it is rather obvious that in the fully dynamic case the symmetry would be broken. No matter whether one approaches the crossover point IV from the left or from the right, the low-loss and thus close-to-laser threshold state will be the one that gets excited. Then, its further evolution will result in either a photonic or excitonic state depending on the direction of encirclement and would have nothing to do with the original state in full agreement with predictions made in Refs. [50–52] and closely related to seminal works of Michael Berry [55,56]. Obviously, implementing dynamic encirclement in polaritonic system would be more difficult than in the case of two modes in the waveguide [54], but if one can rapidly change cavity parameters, the time evolution would follow the path described in recent work [57].

6. DISCUSSION AND CONCLUSIONS

Before concluding, it would be worthwhile to speculate about potential applications of this work. Quite obviously, in the vicinity of the EP, the eigenfrequencies of the two modes diverge rapidly, as has been noted and exploited in Refs. [23–26,58]. For example, in the vicinity of EP2, differentiating over ω_c immediately yields for the split between two

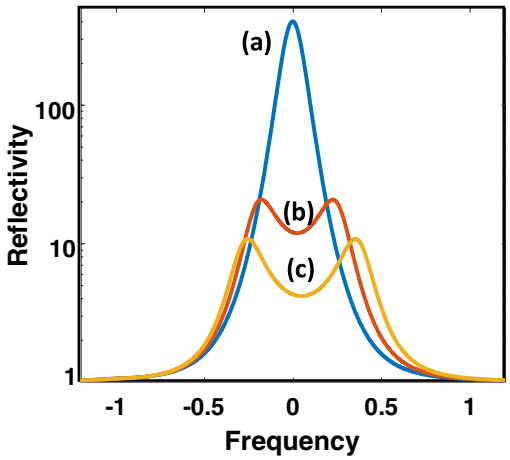

Fig. 9. Reflectivity spectrum of the cavity–exciton system pumped above transparency in the vicinity of the EP: (a) at the EP, (b) cavity frequency shifted by 0.05, and (c) cavity resonant frequency shifted by 0.1.

resonances $\omega_1 - \omega_2 = \Delta\omega\delta(\omega_c)/\sqrt{(\Delta\omega)^2 - \kappa^2}$, and the large change in reflectivity spectrum could be observed as shown in Fig. 9 under the assumption of narrow linewidth (i.e., strong coupling) $\gamma_{21} = \gamma_c = 0.1$; $\Delta\omega = 1$; $\kappa^2 = -1$. As the cavity resonance changes from ω_c to $\omega_c + 0.05$ and then to $\omega_c + 0.1$, the resonance splits and the difference becomes 0.6 and then 0.8, indicating that one can get a "gain" by factor of 10. But, realistically, the measurement would be greatly impeded by the noise coming from amplified spontaneous emission and by the fact that the intensity of the reflected light also changes by more than an order of magnitude. So, while the sensitivity will be improved, the detectivity (which is what really matters) not necessarily so. Furthermore, the fact that the response is nonlinear will greatly limit the dynamic range of the measurement setup. Therefore, at this point, speculation of practical applications should remain just that—speculation in anticipation of further research and ensuing breakthroughs.

The real (if modest) significance of the work described here is in showing that in order to observe PT symmetry and EPs it is absolutely not necessary to contrive a special apparatus with two or more coupled modes for the sole purpose of observation and ensuing knowledge dissemination in publications as is customarily being done. Far from that, a well-studied (one may even say studied to the point of exhaustion) cavity–exciton system, widely known as either cavity polariton or optically pumped VCSEL, when looked upon from a different angle, offers an opportunity to study all the PT phenomena including enhanced sensitivity near the EP and dynamic effects associated with EP encirclement. Two different kinds of EPs can be observed, depending on whether the system is pumped below or above transparency (but below laser threshold). The most intriguing feature uncovered by this work is that EP can be observed in the system where two coupled modes have strikingly different physical origins and that one can use PT symmetry to adiabatically transform the photons to excitons and vice versa. This work expands the scope of physical systems in which PT symmetry and EP phenomena can be observed and will hopefully further stimulate research in this fecund field.

Funding. National Science Foundation Directorate of Engineering (1741694).

Acknowledgment. First, the author acknowledges the stay-at-home and social distancing policies imposed by the authorities in March 2020 for keeping him concentrated on this work, while being shielded from all possible worldly distractions and temptations. Dialogues with Prof. F. Monticone of Cornell University and S. De Liberato of Southampton University have greatly benefited this work. And as always, the opportunity for having stimulating discussions with the co-workers Prof. P. Noir and Dr. S. Artois has been invaluable.

Disclosures. The author declares no conflicts of interest.

REFERENCES

1. C. M. Bender and S. Boettcher, "Real spectra in non-Hermitian Hamiltonians having PT symmetry," Phys. Rev. Lett. **80**, 5243–5246 (1998).
2. C. M. Bender, D. C. Brody, and H. F. Jones, "Complex extension of quantum mechanics," Phys. Rev. Lett. **89**, 270401 (2002).
3. N. Hatano and D. R. Nelson, "Localization transitions in non-Hermitian quantum mechanics," Phys. Rev. Lett. **77**, 570–573 (1996).
4. N. Moiseyev, *Non-Hermitian Quantum Mechanics* (Cambridge University, 2011), p. 394.
5. W. D. Heiss, "Exceptional points of non-Hermitian operators," J. Phys. A **37**, 2455–2464 (2004).
6. D. G. Angelakis, *Quantum Simulations with Photons and Polaritons* (Springer, 2017).
7. E. Yablonovitch, "Inhibited spontaneous emission in solid-state physics and electronics," Phys. Rev. Lett. **58**, 2059–2062 (1987).
8. M. Segev, Y. Silberberg, and D. N. Christodoulides, "Anderson localization of light," Nat. Photonics **7**, 197–204 (2013).
9. L. Lu, J. D. Joannopoulos, and M. Soljačić, "Topological photonics," Nat. Photonics **8**, 821–829 (2014).
10. S. Longhi, "Quantum-optical analogies using photonic structures," Laser Photon. Rev. **3**, 243–261 (2009).
11. A. Ruschhaupt, F. Delgado, and J. G. Muga, "Physical realization of PT-symmetric potential scattering in a planar slab waveguide," J. Phys. A **38**, L171–L176 (2005).
12. R. El-Ganainy, K. G. Makris, D. N. Christodoulides, and Z. H. Musslimani, "Theory of coupled optical PT-symmetric structures," Opt. Lett. **32**, 2632–2634 (2007).
13. K. G. Makris, R. El-Ganainy, D. N. Christodoulides, and Z. H. Musslimani, "Beam dynamics in PT symmetric optical lattices," Phys. Rev. Lett. **100**, 103904 (2008).
14. Z. H. Musslimani, K. G. Makris, R. El-Ganainy, and D. N. Christodoulides, "Optical solitons in PT periodic potentials," Phys. Rev. Lett. **100**, 030402 (2008).
15. A. Guo, G. J. Salamo, D. Duchesne, R. Morandotti, M. Volatier-Ravat, V. Aimez, G. A. Siviloglou, and D. N. Christodoulides, "Observation of PT-symmetry breaking in complex optical potentials," Phys. Rev. Lett. **103**, 093902 (2009).
16. C. E. Rüter, C. E. Rüter, K. G. Makris, R. El-Ganainy, D. N. Christodoulides, M. Segev, and D. Kip, "Observation of parity–time symmetry in optics," Nat. Phys. **6**, 192–195 (2010).
17. H. Hodaei, M. A. Miri, M. Heinrich, D. N. Christodoulides, and M. Khajavikhan, "Parity-time–symmetric microring lasers," Science **346**, 975–978 (2014).
18. L. Feng, M. Ayache, J. Huang, Y. L. Xu, M. H. Lu, Y. F. Chen, Y. Fainman, and A. Scherer, "Nonreciprocal light propagation in a silicon photonic circuit," Science **333**, 729–733 (2011).
19. A. A. Zyablovsky, A. P. Vinogradov, A. A. Pukhov, A. V. Dorofeenko, and A. A. Lisyansky, "PT-symmetry in optics," Phys. Usp. **57**, 1063–1082 (2014).
20. L. Feng, R. El-Ganainy, and L. Ge, "Non-Hermitian photonics based on parity–time symmetry," Nat. Photonics **11**, 752–762 (2017).
21. J. Wen, X. Jiang, L. Jiang, and M. Xiao, "Parity–time symmetry in optical microcavity systems," J. Phys. B **51**, 222001 (2018).
22. S. Klaiman, U. Guenther, and N. Moiseyev, "Visualization of branch points in PT-symmetric waveguides," Phys. Rev. Lett. **101**, 080402 (2008).
23. M. P. Hokmabadi, A. Schumer, D. N. Christodoulides, and M. Khajavikhan, "Non-Hermitian ring laser gyroscopes with enhanced Sagnac sensitivity," Nature **576**, 70–74 (2019).
24. W. Chen, Ş. K. Özdemir, G. Zhao, J. Wiersig, and L. Yang, "Exceptional points enhance sensing in an optical microcavity," Nature **548**, 192–196 (2017).
25. J. Wiersig, "Enhancing the sensitivity of frequency and energy splitting detection by using exceptional points: application to microcavity sensors for single-particle detection," Phys. Rev. Lett. **112**, 203901 (2014).
26. N. A. Mortensen, N. A. Mortensen, P. A. D. Gonçalves, M. Khajavikhan, D. N. Christodoulides, C. Tserkezis, and C. Wolff, "Fluctuations and noise-limited sensing near the exceptional point of parity-time-symmetric resonator systems," Optica **5**, 1342–1346 (2018).
27. M. Brandstetter, M. Liertzer, C. Deutsch, P. Klang, J. Schöberl, H. E. Türeci, G. Strasser, K. Unterrainer, and S. Rotter, "Reversing the pump dependence of a laser at an exceptional point," Nat. Commun. **5**, 4034 (2014).
28. B. Peng, Ş. K. Özdemir, S. Rotter, H. Yilmaz, M. Liertzer, F. Monifi, C. M. Bender, F. Nori, and L. Yang, "Loss-induced suppression and revival of lasing," Science **346**, 328–332 (2014).
29. M. Liertzer, L. Ge, A. Cerjan, A. D. Stone, H. E. Türeci, and S. Rotter, "Pump-induced exceptional points in lasers," Phys. Rev. Lett. **108**, 173901 (2012).
30. W. Gao, X. Li, M. Bamba, and J. Kono, "Continuous transition between weak and ultrastrong coupling through exceptional points in carbon nanotube microcavity exciton–polaritons," Nat. Photonics **12**, 362–367 (2018).
31. T. Fujita, Y. Sato, T. Kuitani, and T. Ishihara, "Tunable polariton absorption of distributed feedback microcavities at room temperature," Phys. Rev. B **57**, 12428–12434 (1998).
32. M. P. V. Exter, A. K. J. V. Doorn, and J. P. Woerdman, "Effect of spatial filtering on the spontaneous emission spectrum of a sub-threshold VCSEL," IEEE J. Sel. Top. Quantum Electron. **1**, 601–605 (1995).
33. C. Weisbuch, M. Nishioka, A. Ishikawa, and Y. Arakawa, "Observation of the coupled exciton-photon mode splitting in a semiconductor quantum microcavity," Phys. Rev. Lett. **69**, 3314–3317 (1992).
34. Y. Todorov, A. M. Andrews, R. Colombelli, S. De Liberato, C. Ciuti, P. Klang, G. Strasser, and C. Sirtori, "Ultrastrong light-matter coupling regime with polariton dots," Phys. Rev. Lett. **105**, 196402 (2010).
35. Å. M. Lindberg, "Mode frequency pulling in He–Ne lasers," Am. J. Phys. **67**, 350–353 (1999).
36. A. Kavokin, *Microcavities*, 2nd ed. (Series on Semiconductor Science and Technology), (Oxford University, 2017), p. 592.
37. J. Bloch, F. Boeuf, J. M. Gérard, B. Legrand, J. Y. Marzin, R. Planel, V. Thierry-Mieg, and E. Costard, "Strong and weak coupling regime in pillar semiconductor microcavities," Physica E **2**, 915–919 (1998).
38. J. Bloch, T. Freixanet, J. Y. Marzin, V. Thierry-Mieg, and R. Planel, "Giant Rabi splitting in a microcavity containing distributed quantum wells," Appl. Phys. Lett. **73**, 1694–1696 (1998).
39. H. Haug and S. W. Koch, *Quantum Theory of the Optical and Electronic Properties of Semiconductors*, 5th ed. (World Scientific, 2009), p. 469.
40. A. E. Siegman, *Lasers* (University Science Books, 1986), p. 1283.
41. F. Gires and P. Tournois, "Interferometre utilisable pour la compression dimpulsions lumineuses modulees en frequence," Comptes Rendus Hebdomadaires Des Seances De L Academie Des Sciences **258**, 6112 (1964).
42. Y. D. Chong, L. Ge, H. Cao, and A. D. Stone, "Coherent perfect absorbers: time-reversed lasers," Phys. Rev. Lett. **105**, 053901 (2010).
43. H. Deng, G. Weihs, D. Snoke, J. Bloch, and Y. Yamamoto, "Polariton lasing vs. photon lasing in a semiconductor microcavity," Proc. Natl. Acad. Sci. USA **100**, 15318–15323 (2003).
44. G. Weihs, H. Deng, R. Huang, M. Sugita, F. Tassone, and Y. Yamamoto, "Exciton-polariton lasing in a microcavity," Semicond. Sci. Technol. **18**, S386–S394 (2003).
45. O. Latinne, N. J. Kylstra, M. Dörr, J. Purvis, M. Terao-Dunseath, C. J. Joachain, P. G. Burke, and C. J. Noble, "Laser-induced degeneracies involving autoionizing states in complex atoms," Phys. Rev. Lett. **74**, 46–49 (1995).
46. A. A. Mailybaev, O. N. Kirillov, and A. P. Seyranian, "Geometric phase around exceptional points," Phys. Rev. A **72**, 014104 (2005).

47. C. Dembowski, H. D. Gräf, H. L. Harney, A. Heine, W. D. Heiss, H. Rehfeld, and A. Richter, "Experimental observation of the topological structure of exceptional points," Phys. Rev. Lett. **86**, 787–790 (2001).
48. S. B. Lee, J. Yang, S. Moon, S. Y. Lee, J. B. Shim, S. W. Kim, J. H. Lee, and K. An, "Observation of an exceptional point in a chaotic optical microcavity," Phys. Rev. Lett. **103**, 134101 (2009).
49. T. Gao, E. Estrecho, K. Y. Bliokh, T. C. H. Liew, M. D. Fraser, S. Brodbeck, M. Kamp, C. Schneider, S. Höfling, Y. Yamamoto, and F. Nori, "Observation of non-Hermitian degeneracies in a chaotic exciton-polariton billiard," Nature **526**, 554–558 (2015).
50. R. Uzdin, A. Mailybaev, and N. Moiseyev, "On the observability and asymmetry of adiabatic state flips generated by exceptional points," J. Phys. A **44**, 435302 (2011).
51. T. J. Milburn, J. Doppler, C. A. Holmes, S. Portolan, S. Rotter, and P. Rabl, "General description of quasiadiabatic dynamical phenomena near exceptional points," Phys. Rev. A **92**, 052124 (2015).
52. I. Gilary, A. A. Mailybaev, and N. Moiseyev, "Time-asymmetric quantum-state-exchange mechanism," Phys. Rev. A **88**, 010102 (2013).
53. A. U. Hassan, B. Zhen, M. Soljačić, M. Khajavikhan, and D. N. Christodoulides, "Dynamically encircling exceptional points: exact evolution and polarization state conversion," Phys. Rev. Lett. **118**, 093002 (2017).
54. J. Doppler, A. A. Mailybaev, J. Böhm, U. Kuhl, A. Girschik, F. Libisch, T. J. Milburn, P. Rabl, N. Moiseyev, and S. Rotter, "Dynamically encircling an exceptional point for asymmetric mode switching," Nature **537**, 76–79 (2016).
55. M. V. Berry, "Optical polarization evolution near a non-Hermitian degeneracy," J. Opt. **13**, 115701 (2011).
56. M. V. Berry and R. Uzdin, "Slow non-Hermitian cycling: exact solutions and the Stokes phenomenon," J. Phys. A **44**, 435303 (2011).
57. C. Wolff, C. Tserkezis, and N. A. Mortensen, "On the time evolution at a fluctuating exceptional point," Nanophotonics **8**, 1319–1326 (2019).
58. J. Wiersig, "Robustness of exceptional-point-based sensors against parametric noise: the role of Hamiltonian and Liouvillian degeneracies," Phys. Rev. A **101**, 053846 (2020).